Available online at www.sciencedirect.com
SCIENCE DIRECT®
Journal of Nuclear Materials 337–339 (2005) 951–955
journal of nuclear materials
www.elsevier.com/locate/jnucmat

Formation of a surface alloy in the beryllium–tungsten system

A. Wiltner *, Ch. Linsmeier *

Max-Planck-Institut für Plasmaphysik, EURATOM Association, Boltzmannstr. 2, D-85748 Garching b. München, Germany

Abstract

The interaction of beryllium and tungsten is investigated by deposition of thin beryllium layers (several nanometers) from the vapor phase onto polycrystalline tungsten substrates and analysis by means of X-ray photoelectron spectroscopy (XPS). Already after room temperature deposition we observe formation of a surface alloy, limited to the interface between the layer and the substrate. The alloy intensity increases continuously between 670 K and 1070 K. The alloy formation is restricted to a depth of 1.2 nm in maximum. Be in excess to this layer thickness desorbs from the sample surface. No Be diffusion or dissolution in the W bulk is observed. Sputter depth profiles before and after annealing experiments in combination with TRIDYN calculations demonstrate that Be is limited to the near-surface area of the tungsten substrate.

PACS: 68.35.−p; 71.20.Lp; 74.70.Ad; 82.80.Pv
Keywords: Beryllium; Tungsten; Surface analysis

1. Introduction

For future fusion devices (e.g. ITER) currently three elements are considered as wall materials [1]. Tungsten will be used in the divertor region, whereas beryllium lines the main chamber. At the strike points the present design considers carbon (carbon fiber-enforced material). Due to erosion processes, material transport and redeposition, in combination with energy input from the plasma, mixed materials will be formed. The investigation of binary model systems from the constituents of the wall materials is necessary to predict altered physical and chemical properties. We already investigate carbon films on Be and W using XPS as a surface sensitive tool [2,3]. Continuing the measurements of binary systems with respect to their use as wall materials we start to investigate the Be–W system. The Be–W phase diagram exhibits three compounds of known stoichiometry: $Be_{22}W$, $Be_{12}W$ and Be_2W [4]. Beside these compounds there exists a miscibility gap and regions of limited miscibility. Due to our applied experimental procedure we expect, if a reaction occurs, the formation of Be_2W. Besides these phase data, little is known in literature about the reactivity of Be and W. Especially XPS measurements which can reveal the alloy formation with high sensitivity are performed for the first time.

2. Experimental

The measurements are performed in an ultrahigh vacuum chamber consisting of an analysis and a preparation system. The analysis system (commercial PHI

* Corresponding authors. Tel.: +49 89 329 922 85; fax: +49 89 329 911 49.
E-mail address: linsmeier@ipp.mpg.de (Ch. Linsmeier).

0022-3115/$ - see front matter © 2004 Elsevier B.V. All rights reserved.
doi:10.1016/j.jnucmat.2004.08.021

ESCA 5600 system, base pressure $1-2\times10^{-8}$ Pa) is equipped with a standard (Mg Kα and Al Kα) and a monochromatic X-ray source (Al Kα, $h\nu = 1486.6$ eV). All measurements shown here are performed using the monochromatic X-ray source. We use pass energies of 93.9 eV for survey scans and 2.95 eV for high resolution measurements. The analysis spot is 0.8 mm in diameter and the energy resolution of the spectrometer system is 0.26 eV. We refer the binding energy scale to the Au $4f_{7/2}$ peak position at 84.0 eV. Furthermore, the analysis chamber is equipped with an ion gun (Specs IQE 12/38) for sample preparation. The polycrystalline tungsten samples are cleaned using alternating sputter (3 kV Ar^+) and annealing cycles (up to 970 K) until no impurities can be detected in the survey scans.

The film deposition is performed in a preparation chamber which is connected to the analysis system. We use a commercial electron beam evaporator (Omicron EFM3) and evaporate Be pieces (HEK GmbH, 99.999%) from a BeO crucible. During the deposition procedure the base pressure is better than 4×10^{-8} Pa. Due to the high reactivity of Be and O the deposited Be films contain a maximum oxygen contamination of 10%.

The experimental procedure is as follows. We deposit Be layers of different thicknesses (from a monolayer up to several nanometers) at room temperature followed by XPS analysis using survey and high resolution scans. The maximum layer thickness in our experiment is limited by the escape depths of the photoelectrons which are in the order of several nanometers. Annealing experiments are performed in two different ways. In procedure I the films are annealed in steps of 100 K up to 1070 K for 30 min per temperature step. The samples are measured by XPS after cooling down to room temperature. In procedure II the samples are annealed at 770, 870 and 970 K for several hours at each temperature while performing XPS analysis at the elevated temperatures. After the long term annealing steps sputter depth profiles (3 kV Ar^+, 45°) are recorded in order to analyze the Be diffusion depth.

3. Results and discussion

After room temperature deposition the Be layer thickness is determined using the procedure given in [5]. We use the density of metallic Be to calculate a Be layer thickness from the XPS intensities of both the substrate (W 4f) and layer signals (Be 1s). The high resolution spectra allow for the deconvolution of the photoelectron signals in components of different chemical species. Beside O no other impurities are detected in the Be layers. The fit procedures applied to deconvolute the Be 1s and W 4f signals are presented elsewhere [6].

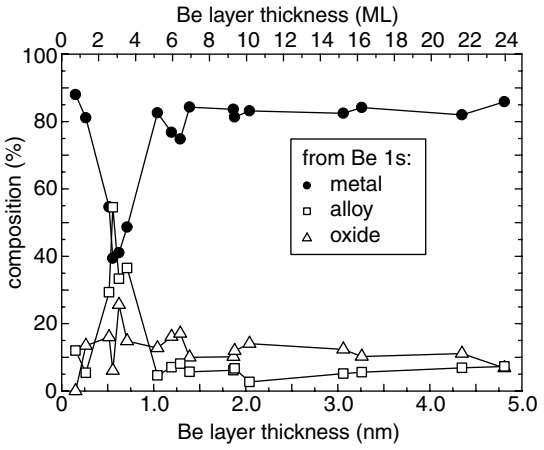

Fig. 1. Composition of Be layers after room temperature deposition. Within the Be 1s signal metallic (●) and oxidic (△) components are identified. Furthermore, a surface alloy (□) which is limited to the interface is observed.

The composition extracted from the Be 1s signal is shown in Fig. 1. Besides the BeO peak at 114.8 eV [7] the Be 1s signal exhibits a peak from metallic Be at 111.8 eV [3] and an additional signal at a lower binding energy of 111.1 eV. Within the substrate signal (W 4f) no oxide signatures (peak shift or broadening) are observed. The oxygen is completely bound to Be. The deconvolution of the W $4f_{7/2}$ signal results in the detection of a peak at 31.0 eV in addition to the peak at 31.4 eV originating from W metal [2]. These two new peaks shifted to lower binding energies compared to the metal signals in both the Be 1s and W 4f transitions are assigned to the formed Be–W surface alloy. As shown in Fig. 1, it is restricted to the interface and additionally deposited Be is predominantly in the metallic state. The oxide fraction is equally distributed in the whole layer and amounts to 10% in average. Due to the small photoemission cross section and therefore low intensity of the Be 1s signal the layer composition below 1 nm (four monolayers) has an error of ±5%. The W 4f substrate signal is dominated by the metallic W intensity from the substrate (>90%). Specifically in this coverage region (up to four monolayers) additional information regarding the layer composition is not obtainable.

3.1. Annealing experiments, procedure I

The layer compositions obtained from high resolution spectra after the annealing steps for two Be films of different initial thicknesses are shown in Fig. 2. In (a) a 1.2 nm thick film is annealed up to 970 K. The layer thickness calculated from the spectrum after the annealing step at 970 K is 1.1 nm. Therefore the Be layer is

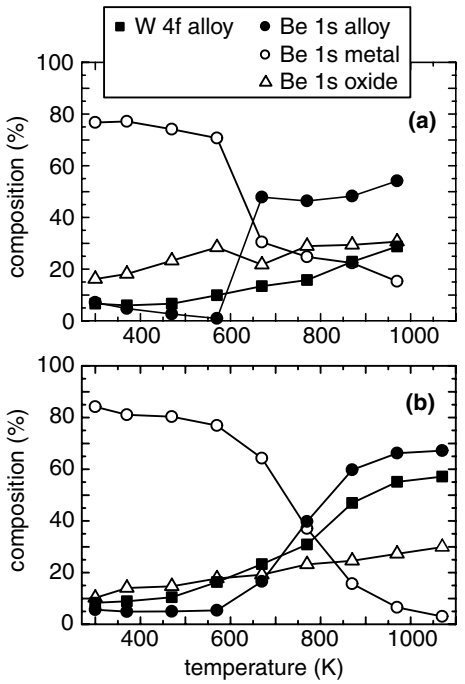

Fig. 2. Thermal behavior (procedure I) of 1.2 nm (a) and 3.3 nm (b) Be films. At 970 K the remaining layer amounts to 1.1 nm (a) and 1.6 nm (b), respectively. After the 1070 K step (b) the Be layer thickness is calculated to 1.4 nm. The alloy fraction intensity increases from 670 K.

stable during the annealing steps. Beginning at 670 K an increase in the alloy fraction is observed within both the Be 1s and W 4f signals. This increase is particularly well visible in the Be 1s signal. Despite the excellent base pressure and due to the high Be–O reactivity the BeO fraction increases slightly with each annealing step. In the substrate signal (W 4f) no oxide fraction is observed. The O 1s signal is broadened and shifted towards higher binding energy values. This observation is in agreement with measurements on the interaction of atomic and molecular O with W and Be surfaces [7].

Annealing of a 3.3 nm Be film leads to a smooth thickness decrease beginning at 570 K. The residual layer at 1070 K amounts to 1.4 nm which is comparable within the experimental precision to the remaining layer thickness of the measurement mentioned above (Fig. 2(a)). The alloy formation is observed in both the substrate and layer signals (Fig. 2(b)). In agreement with the 1.2 nm film the formation of additional Be–W alloy sets in at 670 K. The BeO concentration from the Be 1s signal increases likewise. Furthermore, no oxidic component within the W 4f signal is observed. The O 1s signal is broadened and shifted towards higher binding energy values, as reported above for the 1.2 nm Be film. In both experiments the stoichiometry at 970 K indicates the formation of Be_2W.

3.2. Annealing experiments, procedure II

In order to decide whether Be diffusion or desorption results in a decrease of the initially deposited layer thickness, the Be layers are annealed at elevated temperatures for several hours and subsequently analyzed by XPS sputter depth profiles. During annealing at elevated temperatures the sample composition is analyzed by alternating survey and high resolution scans. Due to the low sensitivity for the Be 1s signal we restrict the high resolution scans to the W 4f signal region. First we consider the changes in the Be layer thickness. The remaining layer thicknesses after the annealing procedures are similar for each experiment and amount to 1.0–1.2 nm, although the initial thicknesses range between 1.1 and 2.0 nm. The Be layer thickness decreases rapidly within the ramp-up to the annealing temperature and stays constant during annealing and after finally cooling down to room temperature.

Fig. 3 summarizes the change during annealing procedures. Fig. 3(a) and (b) shows the W 4f and Be 1s signals, respectively, before and after the 970 K experiment. In the W 4f spectra (3a) the alloy formation leads to the evolution of a second doublet at lower binding energies. The metallic substrate, still present, gives rise to a $W4f_{7/2}$

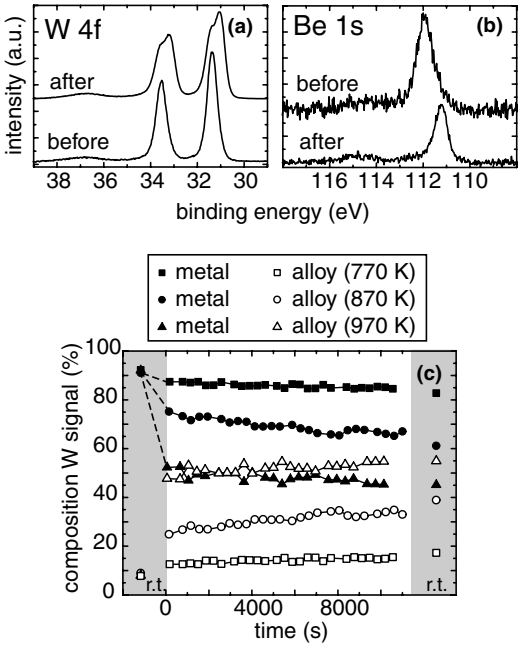

Fig. 3. Substrate (W 4f, a) and layer (Be 1s, b) signals before and after the continuous annealing (procedure II) at 970 K. The alloy formation is visible as an additional doublet (a) and peak shift (b), respectively, within both signals. The composition of the W 4f signal is shown in (c). The reactivity increases with annealing temperature.

peak at 31.4 eV, whereas now the alloy signal intensity at 31.0 eV dominates. The Be 1s peak (3b) shifts completely from the metallic position at 111.8 eV to the alloy signal at 111.1 eV indicating that the total remaining Be is bound in the alloy. As discussed above, a small BeO peak is nevertheless visible at 114.8 eV. The surface compositions obtained from the high resolution spectra in the W 4f region are shown in the central part of Fig. 3(c). The compositions before and after annealing are plotted in the highlighted areas. As indicated by the dashed lines, the bigger part of the alloy formation proceeds already during the ramp-up to the annealing temperatures. Only comparably small additional Be–W alloy is formed during the phases at constant temperatures. At 770 K additional changes are barely visible. At 870 K the alloying reaction proceeds clearly. Within the ramp-up to 970 K the alloy formation increases further, whereas the rate while annealing is comparable to the 870 K run. No alloy decomposition or other compositional changes are observed after cooling to room temperature. In agreement with the annealing experiments conducted by procedure I, the stoichiometry at 970 K indicates the formation of Be_2W.

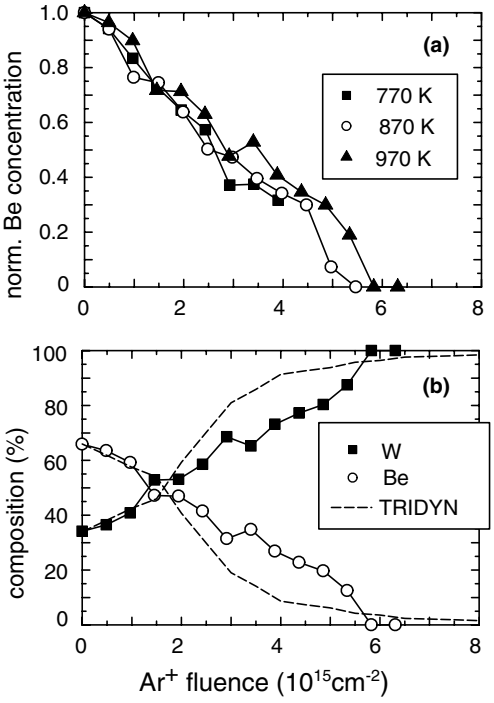

Fig. 4. XPS sputter depth profiles (3 kV Ar^+, 45° incidence) after annealing procedure II at 970 K (see Fig. 3) shown as normalized Be concentration (a). The comparison of a measured depth profile (1.2 nm) with the TRIDYN calculation indicates a limited Be–W intermixing (b).

After the annealing experiments the residual Be–W alloy layers are removed by sputtering while measuring depth profiles by XPS. In Fig. 4(a) the normalized Be depth profiles are plotted. The decrease of Be 1s intensity is comparable for all annealing temperatures, demonstrating equal final alloy layers. Fig. 4(b) shows the depth profile after annealing at 970 K (1.2 nm final Be film thickness) in comparison with a TRIDYN calculation. The TRIDYN code includes a kinematic ion–solid interaction model with a dynamic modification of the sample composition after each collision event [8]. For the TRIDYN calculation the O impurity is neglected. A depth profile of a Be layer, taken after 300 K deposition, shows perfect agreement with TRIDYN results for the measured Be layer thickness (not shown here). The TRIDYN curves in Fig. 4(b) represent a Be layer without intermixing (diffusion, reaction) of Be and W. The slope of the calculated profile is due to ion beam mixing effects and agrees very well with a depth profile of the untreated sample mentioned above [9]. Compared to the depth profile data (after annealing at 970 K) the deviation is small and only significant at fluences between 2 and 5.5×10^{15} $Ar^+ cm^{-2}$. This indicates that the modification of the Be depth distribution during the alloying procedure is small compared to a Be layer of nominally 1.2 nm thickness. The difference between the initially deposited 2.0 nm and the finally calculated 1.2 nm cannot be explained by diffusive Be loss into the W bulk. This would lead to a depth profile where Be extends deeper into the W bulk. The only remaining loss channel for Be is desorption.

4. Summary and conclusions

The Be–W intermetallic system is investigated by depositing thin Be films on polycrystalline tungsten substrates. Analysis of the alloy formation is performed by XPS. Already at room temperature an alloy at the Be–W interface is identified by photoelectron peaks shifted to lower binding energies both in the substrate W 4f and the overlayer Be 1s signals. The alloy signals appear at 111.1 eV (Be 1s) and 31.0 eV ($W 4f_{7/2}$). Despite the well-defined preparation conditions the Be layer contains a small amount of oxygen (approx. 10%) due to the high reactivity of Be. Oxygen is completely bound in BeO, no tungsten oxides are detected. However, the BeO shows no influence on the alloy formation in our experiments. Additional alloying sets in at 670 K, visible in both a decrease in the Be and W metallic peaks and an increase in intensity at the respective alloy binding energies. The alloy formation continues until 970 K where a stoichiometry of Be_2W is reached. The alloy formation at elevated temperatures is limited to a final thickness of approximately 1.2 nm, independent of the initially deposited Be layer thickness. For thicker deposited Be layers, desorption of Be is the proposed loss mechanism,

since sputter depth profiles indicate no Be diffusion into the W substrate. At 970 K, only a slightly widened depth distribution compared to the initial layer is measured. Implications for tungsten fusion first wall components are the decrease in melting point: according to the phase diagram, the Be_2W alloy has a melting temperature of 2500 K, compared to 3690 K of pure tungsten. However, the limited alloying only at the surface, together with the observation of no Be bulk diffusion, indicate that a modification of the tungsten bulk properties is not to be expected. The influence of the alloy formation on the hydrogen isotope retention and re-emission, as well as the changes in surface reactivity towards plasma impurities (carbon and oxygen), will be subject to further studies.

References

[1] R.R. Parker, Nucl. Fusion 40 (2000) 473.
[2] J. Luthin, Ch. Linsmeier, Surf. Sci. 454–456 (2000) 78.
[3] P. Goldstrass, K.U. Klages, Ch. Linsmeier, J. Nucl. Mater. 290–293 (2001) 76.
[4] T.B. Massalski, H. Okamoto, P.R. Subramanian, L. Kacprzak, 2nd Ed., Binary Alloy Phase Diagrams, Materials Park, 1996.
[5] A. Wiltner, Ch. Linsmeier, Phys. Status Solidi A 201 (5) (2004) 881.
[6] A. Wiltner, Ch. Linsmeier, submitted for publication.
[7] Ch. Linsmeier, J. Wanner, Surf. Sci. 454–456 (2000) 305.
[8] W. Eckstein, Springer Ser. Mater. Sci. 10 (1991).
[9] K. Schmid, A. Wiltner, Ch. Linsmeier, Nucl. Instrum. and Meth. B 219&220 (2004) 947.